energies

MDPI

Article

An Experiment and Molecular Dynamics Simulation of Synergistic Foaming between a Surfactant and CO_2 and the Structure–Activity Effect

Lang Zhou [1], Pengfei Chen [2] and Tong Wu [3,*]

[1] Engineering Technology Department, PetroChina Southwest Oil and Gas Field Company, Chengdu 610081, China; zhoulang@petrochina.com.cn
[2] Research Institute of Natural Gas Technology, PetroChina Southwest Oil and Gas Field Company, Chengdu 610213, China; chenpengfei@petrochina.com.cn
[3] State Key Laboratory of Oil and Gas Reservoir Geology and Exploitation, Southwest Petroleum University, Chengdu 610500, China
* Correspondence: 202111000117@stu.swpu.edu.cn

Abstract: CO_2 foam fracturing in tight and shale reservoirs is a revolutionary technique for commercially viable production. Nevertheless, the screening of foaming agents used in CO_2 foam fracturing fluid and the understanding of foaming mechanisms have not been sufficiently investigated. This study aimed to provide a comprehensive method for evaluating and selecting an optimized foaming agent for CO_2 foam fracturing fluid integrating macroscopic and microscopic approaches through laboratory experiments and molecular dynamics simulations. The relationship between the molecular structure of the foaming agent and its corresponding foaming effect was elucidated by taking the interaction between CO_2 and the foaming agent into account. Foam evaluation experiments indicated that the anionic surfactants exhibited superior foaming capacity and inferior stability compared to zwitterionic and non-ionic surfactants. The molecular dynamics simulation results demonstrated that the foaming mechanism of the CO_2 foaming agent relied on the equilibriums between CO_2-surfactant, CO_2-water, and surfactant–water interactions. At the same time, it was found that if the molecular structure of the surfactant contained functional groups that could produce hydrogen bonding with CO_2, the stability of the foaming effect improved to a certain extent, but the foaming volume was not obvious. The classic hydrophilic–lipophilic balance (HLB) theory was not applicable when screening the CO_2 foaming agents. It was found that the ionic surfactants with CO_2-philic groups and linear structures were suitable as the main foaming agents for CO_2 foam fracturing fluids, while non-ionic surfactants with significant steric hindrance were suitable as auxiliary foaming agents. This study provides valuable guidance for selecting cost-effective foaming agents on-site and adds to the understanding of the relationship between the molecular structure of foaming agents and their foaming effects.

Keywords: CO_2 foam fracturing fluid; foaming agent; structure–activity effect; molecular dynamics simulation

Citation: Zhou, L.; Chen, P.; Wu, T. An Experiment and Molecular Dynamics Simulation of Synergistic Foaming between a Surfactant and CO_2 and the Structure–Activity Effect. *Energies* **2024**, *17*, 2465. https://doi.org/10.3390/en17112465

Academic Editor: Franco Berruti

Received: 12 April 2024
Revised: 14 May 2024
Accepted: 16 May 2024
Published: 22 May 2024

1. Introduction

The conventional fossil energy derived from oil and natural gas accounts for a large proportion of energy consumption in various countries, which plays an important role in stabilizing economic development. At present, China's conventional oil and gas resources account for nearly 20%, and are facing many challenges, such as declining production, increasing mining difficulty, and increasing development investment [1]. With the successful development of tight oil in North America, unconventional oil and gas resources have gradually become a new field of oil and gas exploration and development and have attracted more and more attention, which is of great significance to the development of oil and gas

resources in China [2]. Unconventional reservoirs, such as shale oil and gas and tight oil and gas, have development difficulties, such as low porosity, low permeability, and low connectivity. At present, the main stimulation method is hydraulic fracturing [3]. Although hydraulic fracturing mainly uses a more economical slick water fracturing fluid system, the slick water system causes reservoir damage problems, such as water sensitivity in such unconventional oil and gas reservoirs [4,5]. At the same time, it also causes environmental protection problems, such as the waste of water resources in water-deficient areas [6]. The amount of flowback fluid produced after the construction of CO_2 foam fracturing fluid is less, and field treatment is more convenient.

It was found that CO_2 fracturing fluid significantly increases in production after fracturing the reservoir [7]. CO_2 fracturing fluid has the characteristics of low water content and strong diffusivity [8]. Therefore, the reservoir after CO_2 fracturing fluid fracturing has a clear flow channel with complex high conductivity and low damage [9]. At the same time, after CO_2 fracturing, fluid is injected into unconventional reservoirs. CO_2 can promote the desorption of natural gas through competitive adsorption, and CO_2 can also be dissolved in crude oil to improve the fluidity of crude oil [10]. Therefore, CO_2 fracturing fluid is suitable for unconventional natural gas reservoirs with low permeability, strong water sensitivity, and water lock [11].

CO_2 fracturing fluid includes two kinds of water and anhydrous material. The water-free fracturing fluid system is mainly composed of thickener and CO_2, which can completely avoid the damage of water to the reservoir [12]. However, due to the small dielectric constant and low polarizability per unit volume of CO_2, the solubility of solute molecules with large molecular weights or strong polarity is poor, which leads to the difficulty of carrying proppant [13]. Therefore, CO_2 foam fracturing fluid containing water is widely used in the field. It is widely acknowledged that CO_2 foam fracturing fluids exist in an acidic environment. Consequently, the foaming agent must be resistant to adverse reactions with acidic components and maintain stability under such conditions. Hence, foaming agents that are suitable for use with air and nitrogen under neutral conditions may not be appropriate for CO_2 fracturing fluids in acidic environments [14].

Therefore, there is no uniform industry standard for the foaming agent used in CO_2 foam fracturing fluid, and there is still a problem of insufficient understanding of the mechanism. This study aimed to evaluate and select an appropriate foaming agent for CO_2 foam fracturing fluid by adopting a comprehensive approach that encompassed macroscopic and microscopic evaluations through foam evaluation experiments and molecular dynamics simulations. By taking into account the interaction between CO_2 and the foaming agent, we aimed to elucidate the relationship between the molecular structure of the foaming agent and its corresponding foaming effect. This study provides valuable guidance for field personnel in selecting cost-effective foaming agents suitable for industrial applications. Additionally, it contributes to the understanding of the relationship between the molecular structure of foaming agents and their foaming effects, benefiting researchers in this field.

2. Materials and Methods

2.1. Materials

The surfactants utilized in the experiments were commercially available and widely employed in the industry. The materials consisted of Sodium alpha-olefin sulfonate (AOS) [15], Sodium dodecyl benzene sulfonate (SDBS) [16], Sodium alcohol ether sulfate (AES) [17], Sodium laureth sulfate (SLES) [15], *N*-laurylamidopropyl-*N*,*N*-dimethylbetaine (CHSB), and APG0814. All of these surfactants were procured from China National Pharmaceutical Group Chemical Reagent Co., Ltd. (Shanghai, China). The utilized CO_2 gas was acquired from Chengdu Keyuan Gas Co., Ltd. (Chengdu, China), ensuring a purity exceeding 99.9%. The water utilized in the experiments was sourced from a pristine sample collected from an oilfield.

2.2. Experimental

The study involved the Waring blender stirring method to assess the foaming performance of the surfactants [18]. Foam generation was achieved using a high-speed electric stirrer within a high-temperature and high-pressure foam stirring device, as illustrated in Figure 1. The experimental procedure involved preparing a solution of the surfactant with a mass concentration of 0.4%. The solution was then placed in a visual constant temperature drying oven for 8 h. Subsequently, a 100 mL portion of the solution was transferred into a sealed stirring container. Then, CO_2 was used to purge the stirred tank at a constant flow rate for 3 min to eliminate air interference in the tank. The power supply of the stirring device was turned on to shear the stirring solution at a speed of 1000 rpm for 60 s to prepare the foam. The volume change of the foam was continuously observed. Firstly, the maximum value of the foam volume ($V_{\max}$) was recorded, and then the time to reach 0.5 Vmax for the volume of the foam in the measuring cylinder was recorded, which was called the foam half-life ($t_{1/2}$). The time it took for the foam system to precipitate half of the liquid was called the drainage half-life of the liquid. The experiment was repeated by substituting various foaming agents and modifying the experimental temperatures and pressures. Subsequently, the foam volume, foam half-life, drainage half-life, and foam quality were examined to assess the foaming properties of each surfactant.

$$Q_f = \frac{V_{gas}}{V_{all}} \tag{1}$$

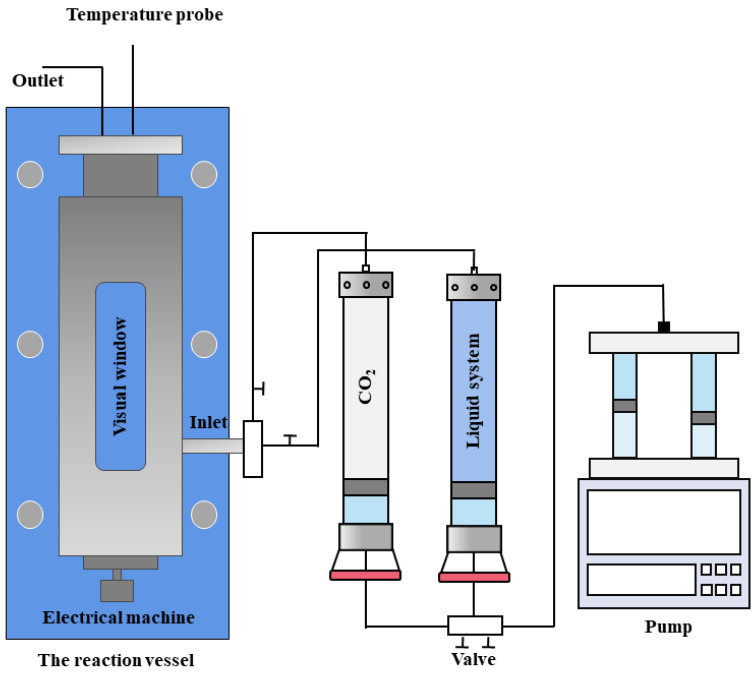

Figure 1. Foam reactor.

Q_f is the foam quality, %. V_{gas} is the gas volume, mL. V_{all} is the total volume of the system, mL.

The measurement of the foaming ability of the surfactants was limited to only three parameters: the foam volume, foam half-life, and drainage half-life. Accordingly, this paper introduced time parameters to provide a comprehensive evaluation of the foam performance. To assess the overall performance of the foam, a comprehensive index (S) was introduced. The calculation formula for the comprehensive index of foam is as follows:

$$S = \frac{1}{2}\left(V_{\max} + \frac{1}{2}V_{\max}\right) \times t_{1/2} = \frac{3}{4}V_{\max}t_{1/2} \tag{2}$$

2.3. Molecular Dynamics Simulation

2.3.1. Model

The three types of periodic systems, namely CO_2, CO_2/surfactant, and CO_2/surfactant/water, were constructed using Materials Studio software 2019. These systems are depicted in Figure 2. The composition of each box is shown in Table 1. System 1 constructed CO_2 molecules as a blank group to verify the applicability of the force field. Systems 2–9 were CO_2 periodic boxes with surfactants, and the interaction between CO_2 and the surfactants was investigated. Systems 10–17 constructed periodic boxes of different types of surfactants and CO_2 under water-bearing conditions and investigated the intermolecular interactions between CO_2 and the surfactants under water-bearing conditions. The COMPASS force field based on an ab initio calculation was used, which was suitable for simulating CO_2 and hydrocarbon systems [19,20].

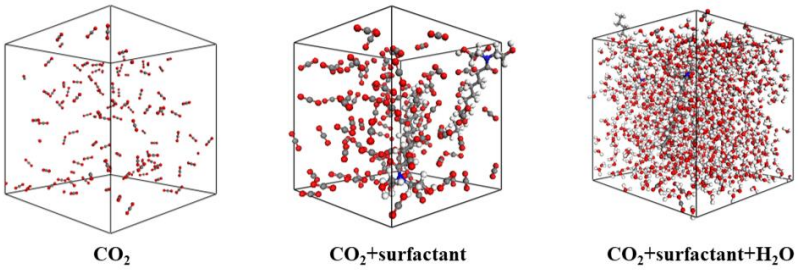

Figure 2. Three periodic models of amorphous molecules.

Table 1. Composition of the molecular dynamics calculation system.

System	Composition	No. of CO_2 Molecules	No. of Surfactant Units	No. of H_2O Molecules
1	CO_2	100	0	0
2	CO_2/AOS	100	2	0
3	CO_2/SDBS	100	2	0
4	CO_2/AES	100	2	0
5	CO_2/SLES	100	2	0
6	CO_2/CHSB	100	2	0
7	CO_2/CAB	100	2	0
8	CO_2/6501	100	2	0
9	CO_2/0814	100	2	0
10	CO_2/AOS/H_2O	100	2	1000
11	CO_2/SDBS/H_2O	100	2	1000
12	CO_2/AES/H_2O	100	2	1000
13	CO_2/SLES/H_2O	100	2	1000
14	CO_2/CHSB/H_2O	100	2	1000
15	CO_2/CAB/H_2O	100	2	1000
16	CO_2/6501/H_2O	100	2	1000
17	CO_2/0814/H_2O	100	2	1000

2.3.2. Process

The molecular dynamics simulation involved the Nosé–Hoover method to control the temperature [21], the Berendsen method to control the pressure [22], the Ewald method to calculate the electrostatic interactions [23]. We calculated the van der Waals interactions based on the atomic sum. The cutoff radius of 15.5 Å was utilized. The molecular dynamics simulation process was as follows:

(1) The initial model was constructed based on the basic physical properties of substances in the National Institute of Standards and Technology (NIST) database, and geometric optimization was performed;

(2) The system underwent 10 cycles of annealing, gradually increasing from 298 to 500 K and then returning to 298 K in order to achieve equilibrium;
(3) When the system was an NPT ensemble, 298 K, 0.1 MPa, and the time step was set to 1 fs, the molecular dynamics simulation process was a total of 5000 ps. The force field verification is shown in Table 2.

Table 2. Density of different fluids (T = 298.15 K, P = 0.1 MPa).

Fluid Type	NIST (g/cm^3)	Value of Simulation (g/cm^3)	Error (%)
H_2O	0.9971	0.9781	1.906%
CO_2	0.0018	0.0017	5.556%

2.3.3. Calculation Method

The interaction between the surfactant and CO_2 was discussed based on parameters such as binding energy, radial distribution function, and cohesive energy density [24].

The binding energy is defined as the energy needed to separate the two substances, indicating the strength of their interaction. A negative binding energy value indicates an attractive force between the two substances. In the MD simulation, the binding energy is calculated as follows [25]:

$$E_{\text{inter}} = E_{\text{all}} - (E_{\text{A}} + E_{\text{B}}) \tag{3}$$

In the formula, E_{inter} is the interaction energy between the substances in the total system, kJ/mol. E_{all} represents the total energy of the system, kJ/mol. E_{A} and E_{B} represent the respective system energies of A and B, kJ/mol.

The radial distribution function (RDF) quantifies the likelihood of finding a second particle at a given distance, r, from a central particle relative to its random distribution. The RDF provides insights into the arrangement and interaction of particles within the system. The RDF is calculated as follows [26]:

$$g_{\alpha\beta}(r) = \frac{V_S}{N_\alpha N_\beta} \sum_{i=1}^{N_\alpha} \frac{n_{i\beta}(r)}{4\pi r^2 \Delta r} \tag{4}$$

In the formula, $n_{i\beta}(r)$ represents the count of β particles within the range (r, $r + \Delta r$) centered on the ith α particle. $g_{\alpha\beta}(r)$ signifies the average probability of β particles appearing within the same range per unit volume, with the α particles as the reference center.

The cohesive energy density (CED) provides a measure of the intermolecular interaction strength within the system. It quantifies the amount of energy required to gasify a unit volume of material. The value of CED corresponds to the system's solubility parameter, indicating the degree of solubility of different substances in the system. The CED is calculated as follows [27]:

$$\begin{cases} CED = \frac{\Delta H_{\text{v}} - RT}{V_{\text{m}}} \\ \delta = \sqrt{CED} = \sqrt{\frac{\Delta H_{\text{v}} - RT}{V_{\text{m}}}} \end{cases} \tag{5}$$

The formula includes the following variables: ΔH_{v}, which represents the molar evaporation heat in kJ/mol; RT, the expansion work performed during the vaporization process in kJ/mol; V_{m}, the molar volume in mol/L; CED, the cohesive energy density in J/m^3; and δ, the solubility parameter in (J/m^3)$^{1/2}$.

3. Results and Discussion

3.1. Foam Properties of Different Surfactants

CO_2 foam refers to a dispersion system where CO_2 gas molecules are dispersed in water. In this system, CO_2 acts as the dispersed phase, while water serves as the dispersion medium. Consequently, CO_2 foam represents an inherently unstable thermodynamic system, tending towards reaching a state-of-energy equilibrium. From a macro point of view, the whole foam system is stable, or the foam system bursts. To select a suitable

foaming agent for CO_2, factors such as foam quality, foam half-life, and drainage half-life of the entire system were considered during the screening process.

The analysis of Figure 3a reveals a decrease in the foaming volume for each surfactant as time progresses, following an exponential decay pattern. Once the foam is generated, it undergoes uneven liquid film flow due to the combined effects of gravity and pressure gradients. Additionally, the gas within the foam continues to diffuse and permeate through the foam film, driven by the pressure disparities between its two sides [28]. The gas diffusion through the liquid film and the liquid film drainage only play an obvious role in the initial stage of the formation of the foam system. As the foam system decays, the above two effects gradually weaken, making the foam decay rate gradually slow down.

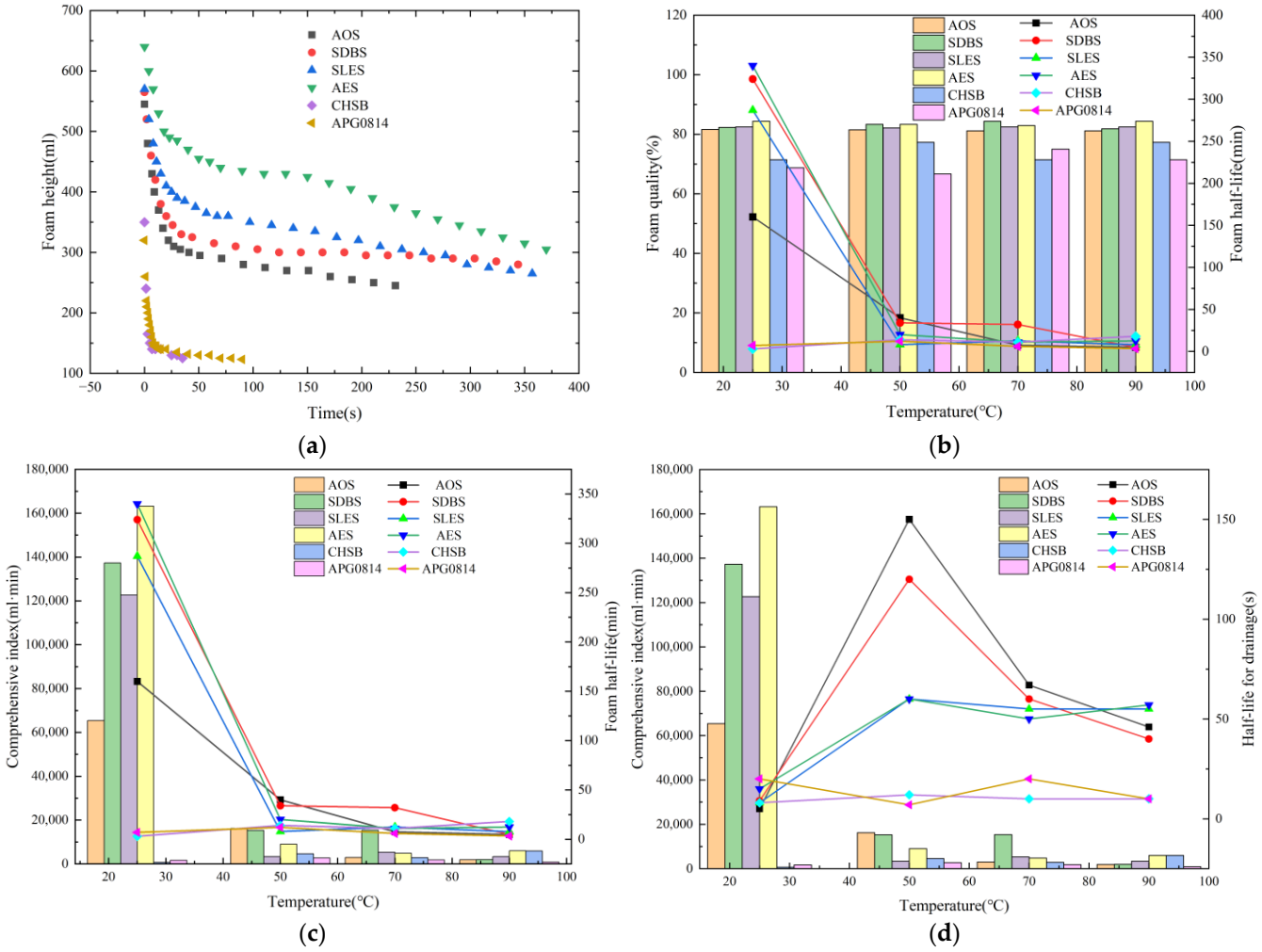

Figure 3. Effect of temperature on the foaming properties of different surfactants. (**a**) Bubble decline; (**b**) Foam half-life/foam quality; (**c**) Foam half-life/compositive index; (**d**) Compositive index/Foam half-life for drainage.

From Figure 3b–d, it can be seen that the foaming volume and half-life of each foaming agent decrease with the increase in temperature, and the stability of the foam decreases strongly. At the same time, it was found that ionic surfactants changed more dramatically than zwitterionic and non-ionic surfactants. At the bubble interface (plateau interface), surfactant molecules are adsorbed on the surface of water. The repulsion between the polar groups of the surfactant makes the adsorbed molecules maintain a certain molecular exclusive area [29]. At low heating rates, molecular thermal motion enhances intermolecular interactions and prolongs the initial half-life of liquation, although the foam half-life remains shorter. At high temperatures, the change in electrical repulsion is minimal, but

the increase in temperature intensifies molecular thermal motion, thereby affecting the adsorption state of the surfactant molecules at the interface. Hence, ionic surfactants exhibit lower stability compared to other types.

Figure 4 reveals a gradual and weak decrease in the foaming volume of each foam system as the pressure increases. Applying pressure to the foaming environment significantly prolongs the foam's lifespan compared to normal pressure conditions. According to the Laplace equation, the gas pressure within small bubbles exceeds that of larger bubbles, creating a pressure gradient that causes gas from small bubbles to migrate into larger bubbles through the liquid film. As a result, the small bubbles gradually diminish and vanish, while the large bubbles progressively expand until they rupture. The more uneven the bubble size distribution is, the worse the foam stability is. On the contrary, the more uniform the bubble size is, the more stable the foam is, which is consistent with the theoretical analysis of Monsalve [30]. Therefore, this paper argues that the pressure has little effect on the foaming volume of the foam system but has a significant effect on the stability of the foam system, and the pressure is beneficial in improving the stability of the CO_2 foam.

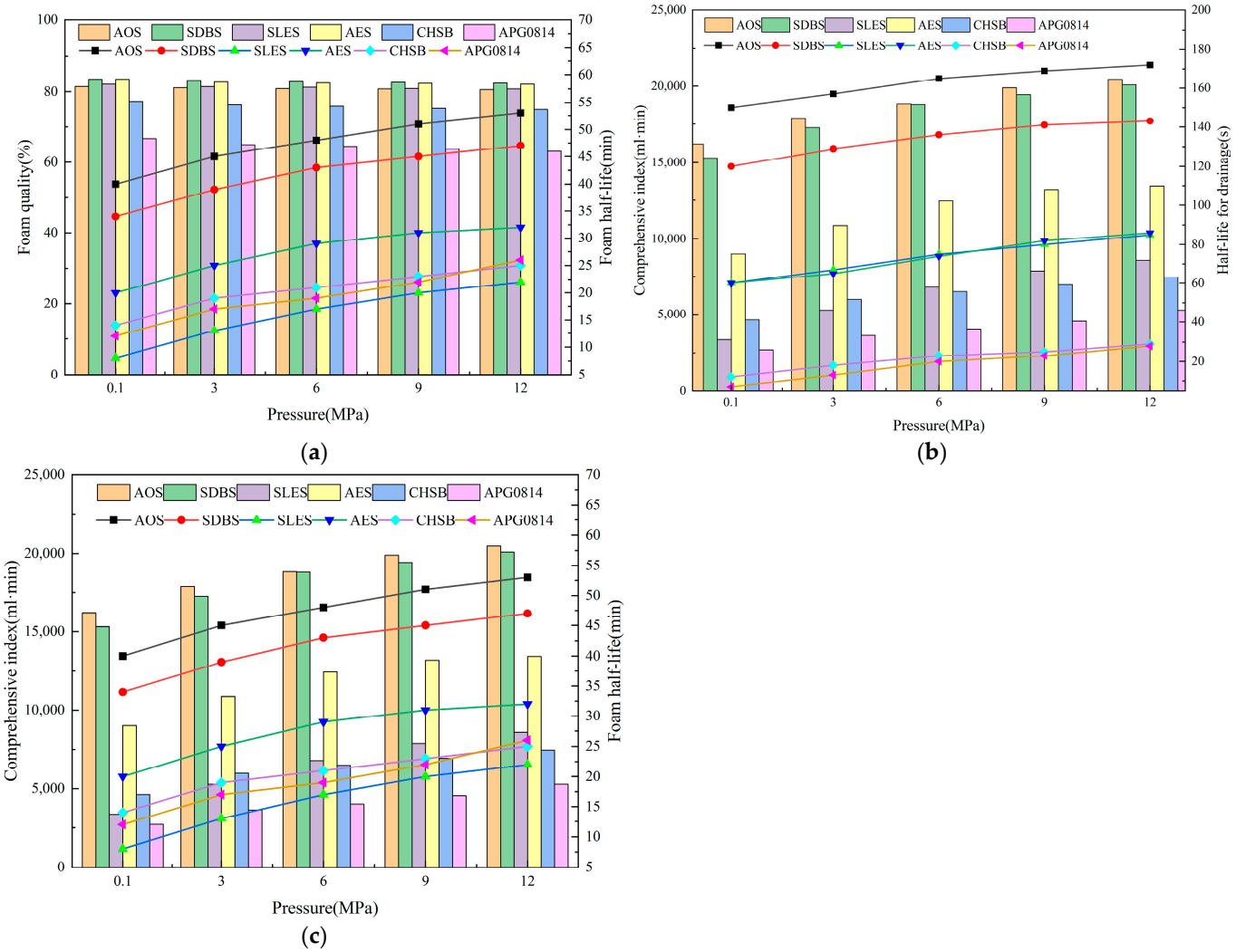

Figure 4. Effect of pressure on the foaming properties of different surfactants. (**a**) Foam half-life/foam quality; (**b**) Compositive index/Foam half-life for drainage; (**c**) Foam half-life/compositive index.

The experimental results reveal that non-ionic and zwitterionic surfactants exhibit better stability than anionic surfactants. However, their half-life and foam quality are significantly inferior to those of anionic surfactants. Additionally, the overall foaming properties of SDBS, AES, and SLES are similar, but AES and SLES demonstrate greater

stability than SDBS. The key distinguishing feature among the three is the presence of an ethylene oxide (EO) structure in their molecular chains.

The analysis reveals that the EO group exhibits hydrophilicity, and as the degree of polymerization of the EO group increases, the hydrophilicity of the surfactant also enhances. Consequently, this leads to an expansion of the exclusive adsorption area at the interface, a reduction in the surface tension at the critical micelle concentration, and a decrease in the foam system's surface energy, all of which contribute to enhancing the stability of the entire foam system. In cases where the hydrophobic groups in the surfactant molecules share similarities, the degree of polymerization of the EO group directly impacts the volume of the hydration layer surrounding the molecule. Consequently, a higher degree of polymerization results in a larger hydration layer volume, leading to increased repulsive forces between the foam formations. This subsequently decreases the drainage rate of the liquid film, ultimately delaying the rupture process of the foam's liquid film. At the same time, the increase in the EO polymerization degree is beneficial to enhance the interaction between the surfactant molecules, promote the more uniform arrangement of the surfactant molecules on the surface of the water film, increase the strength of the liquid film, and improve the stability of the foam. Therefore, it is considered that the surfactant-containing EO group is beneficial to foaming in a CO_2 environment, which is consistent with the results of others [31].

3.2. The Interaction between the Surfactant and CO_2

This section addresses the CO_2-surfactant interaction and presents a qualitative evaluation using the intermolecular interaction energy, radial distribution function, and solubility parameter. Figure 5 shows the interaction between CO_2 and the surfactant. The results indicated that the interaction energy between the ionic surfactants and CO_2 was stronger than that of non-ionic surfactants. This is attributed to the presence of a pair of lone electrons on the CO_2 molecule, which strengthens the non-bond interaction with ionic surfactants.

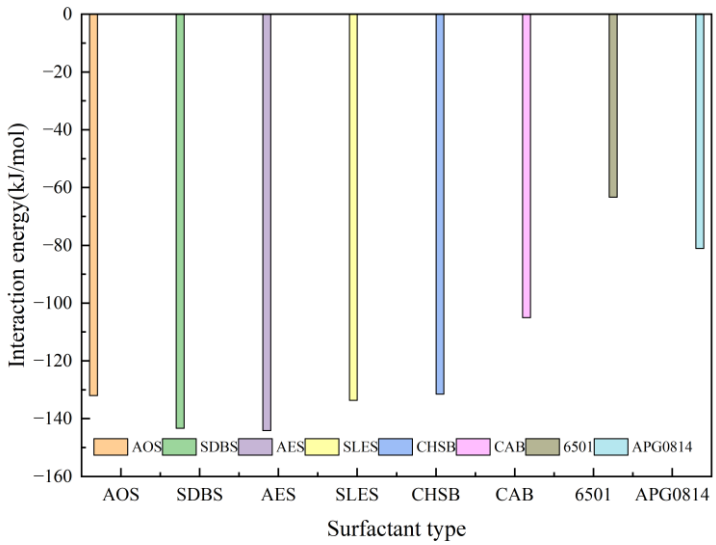

Figure 5. The binding energy between CO_2 and the surfactant.

Figure 6 illustrates the radial distribution function calculated for CO_2 and surfactant molecules. It allows for a qualitative examination of the distribution and arrangement of CO_2 around the surfactant. The peak position in the radial distribution function indicates the type of interaction. Short-range interactions between molecules typically comprise hydrogen bonding (<3.5 Å) and van der Waals interactions (3.5–5.0 Å), whereas long-range interactions generally involve electrostatic interactions (>5.0 Å) [27]. Figure 6 reveals that the first peak position of 6501 and APG0814 was less than 3.5 Å. This can be attributed to the presence of amide bonds in 6501 and hydroxyl groups in APG0814. The interaction

between the CO_2 molecules and these two surfactants was facilitated by the formation of hydrogen bonds, resulting in CO_2 being distributed in two layers around them. On the other hand, the interaction of CO_2 with other surfactants was predominantly governed by van der Waals forces. Given the non-polar nature of CO_2, its mutual attraction with the surfactants is primarily driven by dispersion forces.

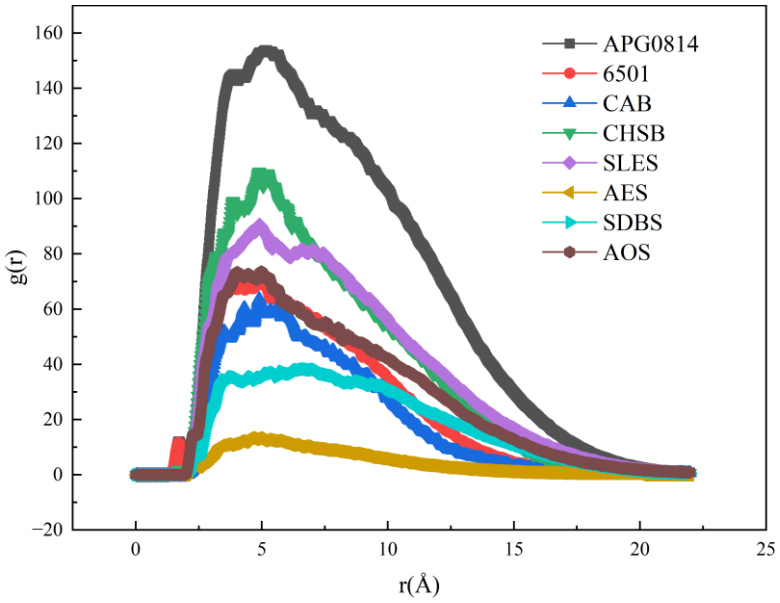

Figure 6. Radial distribution function between CO_2 and the surfactant.

The cohesive energy density of each surfactant system was determined using a molecular dynamics simulation, and the results are presented in Table 3. Generally, a higher polarity of the functional groups within the molecule leads to increased intermolecular forces and corresponding cohesive energy density. The results in Table 3 demonstrate that electrostatic interactions dominated the cohesive energy density between the CO_2 molecules and ionic surfactant molecules, with the anionic surfactant exhibiting greater strength compared to the zwitterionic surfactant. The cohesive energy density between the CO_2 molecules and non-ionic surfactant molecules did not exhibit a dominant force, with both the van der Waals force and electrostatic force making comparable contributions.

Table 3. Cohesive energy density and solubility parameters between CO_2 and various surfactants.

System	E_{van} /(J/m^3)	E_{elect} /(J/m^3)	E_{other} /(J/m^3)	CED /(J/m^3)	δ /(J/m^3)$^{1/2}$
CO_2 + AOS	1.627×10^6	6.443×10^6	5.611×10^2	8.071×10^6	2.841
CO_2 + SDBS	1.377×10^7	5.611×10^7	3.612×10^4	6.992×10^7	8.362
CO_2 + AES	3.333×10^6	9.807×10^6	6.459×10^3	1.315×10^7	3.626
CO_2 + SLES	3.321×10^6	1.292×10^7	1.896×10^3	1.624×10^7	4.030
CO_2 + CHSB	4.04×10^6	6.832×10^6	2.266×10^3	1.087×10^7	3.298
CO_2 + CAB	2.291×10^6	3.394×10^6	7.407×10^2	5.686×10^6	2.385
CO_2 + 6501	3.732×10^5	3.509×10^5	7.836×10^1	7.241×10^5	0.851
CO_2 + 0814	5.843×10^5	6.006×10^5	9.381×10^1	1.185×10^6	1.089

3.3. The Interaction between the Surfactant and CO_2 under Aqueous Conditions

This section explores the interaction between CO_2 and the surfactants in aqueous conditions, including a qualitative evaluation using binding energy, radial distribution function, and cohesive energy density. Figure 7 illustrates the interaction between CO_2 and the surfactant under water-bearing conditions. There was a general belief that a larger absolute value of the interaction energy signified a stronger attraction between the

surfactant and the entire system, leading to a higher possibility of miscibility with CO_2. It was found that the interaction energy between the ionic surfactants and CO_2 was stronger than that of the non-ionic surfactants, which was consistent with the results found in Section 3.2. The strongest interaction between the surfactant–CO_2-water system was SLES and the weakest was 6501. Therefore, considering the intermolecular binding energy, ionic surfactants were better suited as foaming agents for CO_2. At the same time, it was observed that the interaction energy between the ionic surfactants with a simple linear structure was greater than that of the non-ionic surfactants with substantial steric hindrance.

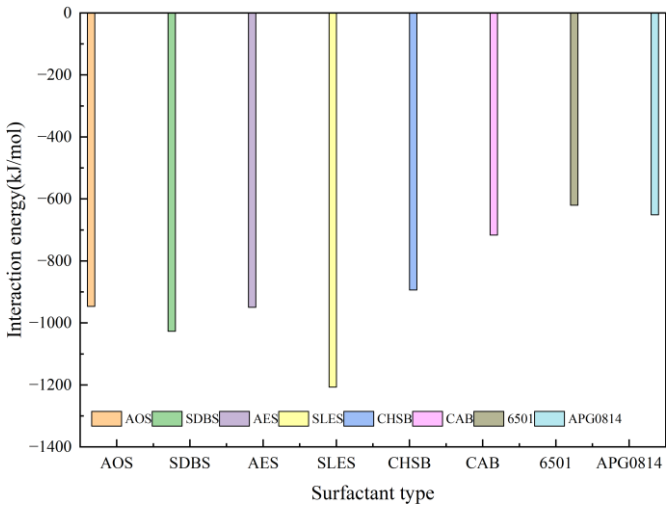

Figure 7. Interaction energy between CO_2, the surfactant, and water.

The distribution of the CO_2 molecules around the surfactant molecules in different surfactant systems under water-containing conditions was studied, as shown in Figure 8. It can be seen from Figure 8 that the peak position of the CO_2 and surfactant in each surfactant system was greater than five, and the interaction between the two was mainly the long-range electrostatic force, which was a weak interaction. A comparison of the radial distribution function results between 6501 and APG0814 in Section 3.2 revealed the absence of hydrogen bonds in groups such as the amide and hydroxyl groups, which are known for their propensity to form hydrogen bonds as a result of water presence. The radial distribution function results for each surfactant showed minimal variation, indicating weak CO_2-surfactant interactions in all mixed systems. However, the peak value of the ionic surfactants was generally higher than that of the non-ionic surfactants, indicating a better potential for a foaming effect.

The cohesive energy density of each system was obtained via a molecule dynamics simulation, and the results are shown in Table 4. It can be seen from Table 4 that, similar to the results in Section 3.2, the cohesive energy density between CO_2 and the ionic surfactants was dominated by electrostatic force interactions. The difference was that there was no dominant force in the cohesive energy density of the CO_2 molecules and zwitterionic surfactants, and the contribution of van der Waals forces and electrostatic forces was similar. CO_2 can be used as both a Lewis base and Lewis acid, which leads to the similar contribution of the electrostatic interactions and van der Waals interactions of zwitterionic surfactants.

Surfactants can reduce the interfacial tension (IFT) between CO_2 and the water phase, thereby increasing the resistance of liquid precipitation in the foam liquid film and enhancing the stability of the foam. Some surfactants with long chains can increase the viscosity of the foam liquid film, slow down the liquid precipitation, reduce the bubble coalescence phenomenon, and further improve the foam stability. In addition, the CO_2-philic groups of surfactants, such as the ester and ether groups, can increase the interaction with CO_2 and increase the length of the chain segment, affecting the distribution of the molecules at the interface. The confinement effect of surfactant adsorption at the interface may limit the

movement of CO_2 at the interface and promote the growth of interface thickness, which affects the diffusion coefficient of CO_2.

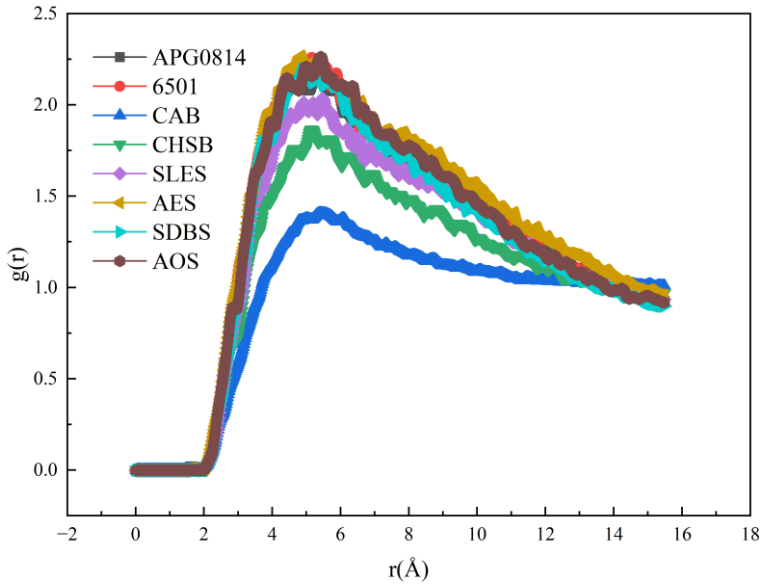

Figure 8. The radial distribution function of the surfactant–CO_2 system under water conditions.

Table 4. The whole system of cohesive energy density and the solubility parameters.

System	E_{van} /(J/m^3)	E_{elect} /(J/m^3)	E_{other} /(J/m^3)	CED /(J/m^3)	δ /(J/m^3)$^{1/2}$
CO_2 + AOS + H_2O	0.377×10^9	1.734×10^9	2.982×10^6	2.114×10^9	45.978
CO_2 + SDBS + H_2O	0.376×10^9	1.864×10^9	3.369×10^6	2.280×10^9	47.751
CO_2 + AES + H_2O	0.382×10^9	1.808×10^9	3.316×10^6	2.213×10^9	47.042
CO_2 + SLES + H_2O	0.404×10^9	1.851×10^9	3.344×10^6	2.259×10^9	47.534
CO_2 + CHSB + H_2O	1.061×10^9	1.069×10^9	3.292×10^6	2.133×10^9	46.180
CO_2 + CAB + H_2O	1.122×10^9	1.086×10^9	3.396×10^6	2.211×10^9	47.02
CO_2 + 6501 + H_2O	1.091×10^9	1.095×10^9	3.343×10^6	2.186×10^9	46.758
CO_2 + 0814 + H_2O	1.005×10^9	1.01×10^9	2.973×10^6	2.014×10^9	44.881

Furthermore, no consistent relationship was observed between the hydrophilic–lipophilic balance (HLB) values and solubility parameters. The HLB values for AOS [32], SDBS [33], AES [34], SLES [35], CHSB [28], CAB [36], 6501 [37], and APG0814 were 15.4, 10.6, 14, 14, 8.7, 13.48, 14, and 12.45, respectively.

4. Conclusions

This study initially evaluated and selected surfactants suitable for CO_2 environments through foaming experiments and explored the impact of temperature and pressure on the stability of the foam. Subsequently, molecular dynamics simulations were employed to investigate the interactions between CO_2 and the surfactants, as well as CO_2, the surfactants, and water. The study compared the binding energy, radial distribution functions, and solubility parameters of different CO_2-surfactant systems in CO_2 environments, which are crucial factors for foaming effects, and discussed the influence of molecular structures on these interactions. The conclusions drawn are as follows:

1. Compared to non-ionic surfactants with certain steric hindrance, ionic surfactants with a simple linear structure exhibit better foaming performance but poorer foam stability. Concurrently, high temperatures are detrimental to the stability of CO_2 foam, while higher pressures are beneficial;

2. The mechanism of action of CO_2 foaming agents depends on the balance among the interactions between CO_2 and surfactant molecules, CO_2 and water molecules, and the surfactant and water molecules. All substances formed dispersed systems of various aggregates in water rather than simply dissolving;
3. Classical hydrogen bonding theories and the HLB (hydrophilic–lipophilic balance) theory are not applicable to the selection of CO_2 foaming agents. It was found that the presence of EO (ethylene oxide) groups, which are CO_2-philic, is advantageous for foaming in CO_2 environments, and the formation of hydrogen bonds can enhance the stability of CO_2 foam.

This paper has certain limitations as it does not account for the synergistic effect of different surfactants. Future research will be focused on the correlation between the molecular structure and foaming performance of synergistic foaming agents.

Author Contributions: Conceptualization, L.Z., P.C. and T.W.; Methodology, P.C.; Writing—original draft, T.W.; Funding acquisition, L.Z. and P.C. All authors have read and agreed to the published version of the manuscript.

Funding: This research was funded by the Science and Technology Project of PetroChina Southwest Oil and Gas Field Company (20230302-33).

Data Availability Statement: The original contributions presented in the study are included in the article, further inquiries can be directed to the corresponding author.

Conflicts of Interest: Authors Lang Zhou and Pengfei Chen were employed by the PetroChina Southwest Oil and Gas Field Company. The remaining authors declare that the research was conducted in the absence of any commercial or financial relationships that could be construed as a potential conflict of interest.

References

1. Tong, X.; Zhang, G.; Wang, Z.; Wen, Z.; Tian, Z.; Wang, H.; Ma, F.; Wu, Y. Distribution and Potential of Global Oil and Gas Resources. *Pet. Explor. Dev.* **2018**, *45*, 779–789. [CrossRef]
2. Zhao, J.; Ren, L.; Jiang, T.; Hu, D.; Wu, L.; Wu, J.; Yin, C.; Li, Y.; Hu, Y.; Lin, R.; et al. Ten years of Gas Shale Fracturing in China: Review and Prospect. *Nat. Gas Ind. B* **2022**, *9*, 158–175. [CrossRef]
3. Lei, Q.; Yang, L.; Duan, Y.; Weng, D.; Wang, X.; Guan, B.; Wang, Z.; Guo, Y. The "Fracture-Controlled Reserves" Based Stimulation Technology for Unconventional Oil and Gas Reservoirs. *Pet. Explor. Dev.* **2018**, *45*, 770–778. [CrossRef]
4. Lei, Q.; Weng, D.; Xiong, S.; Liu, H.; Guan, B.; Deng, Q.; Yan, X.; Liang, H.; Ma, Z. Progress and Development Directions of Shale Oil Reservoir Stimulation Technology of China National Petroleum Corporation. *Pet. Explor. Dev.* **2021**, *48*, 1198–1207. [CrossRef]
5. Barati, R.; Liang, J.-T. A Review of Fracturing Fluid Systems Used for Hydraulic Fracturing of Oil and Gas Wells. *J. Appl. Polym. Sci.* **2014**, *131*, 40735. [CrossRef]
6. Mian, C.; Hongkui, G.; Jinzhou, Z.; Jun, Y. The Key Fundamentals for the Efficient Exploitation of Shale Oil and Gas and Its Related Challenges. *Pet. Drill. Tech.* **2015**, *43*, 7–14.
7. Burke, L.H.; Nevison, G.W.; Peters, W.E. Improved Unconventional Gas Recovery with Energized Fracturing Fluids: Montney Example. In Proceedings of the SPE Eastern Regional Meeting, Columbus, OH, USA, 17 August 2011; p. SPE-149344-MS.
8. Zhang, C.; Pathegama Gamage, R.; Perera, M.; Zhao, J. Characteristics of Clay-Abundant Shale Formations: Use of CO_2 for Production Enhancement. *Energies* **2017**, *10*, 1887. [CrossRef]
9. Zhang, C.P.; Liu, S.; Ma, Z.Y.; Ranjith, P.G. Combined Micro-Proppant and Supercritical Carbon Dioxide (SC-CO_2) Fracturing in Shale Gas Reservoirs: A review. *Fuel* **2021**, *305*, 121431. [CrossRef]
10. Guo, J.; Li, M.; Cong, L. Progress and development directions of fracturing flooding technology for tight reservoirs in China. *Acta Pet. Sin.* **2022**, *43*, 1788.
11. Wang, H.; Li, G.; He, Z.; Shen, Z.; Li, X.; Zhang, Z.; Wang, M.; Yang, B.; Zheng, Y.; Shi, L. Analysis of mechanisms of supercritical CO_2 fracturing. *Rock Soil Mech.* **2018**, *39*, 3589–3596.
12. Sun, X.; Dai, C.; Sun, Y.; Du, M.; Wang, T.; Zou, C.; He, J. Wettability Alteration Study of Supercritical CO_2 Fracturing Fluid on Low Permeability Oil Reservoir. *Energy Fuels* **2017**, *31*, 13364–13373. [CrossRef]
13. Prasad, S.K.; Sangwai, J.S.; Byun, H.-S. A Review of the Supercritical CO_2 Fluid Applications for Improved Oil and Gas Production and Associated Carbon Storage. *J. CO2 Util.* **2023**, *72*, 102479. [CrossRef]
14. Abdelaal, A.; Aljawad, M.S.; Alyousef, Z.; Almajid, M.M. A Review of Foam-Based Fracturing Fluids Applications: From Lab Studies to Field Implementations. *J. Nat. Gas Sci. Eng.* **2021**, *95*, 104236. [CrossRef]

15. Ahmed, S.; Elraies, K.A.; Hanamertani, A.S.; Hashmet, M.R.; Shafian, S.R.; Hsia, I.C. Investigation of Carbon Dioxide Foam Performance Utilizing Different Additives for Fracturing Unconventional Shales. In Proceedings of the Abu Dhabi International Petroleum Exhibition and Conference, Abu Dhabi, United Arab Emirates, 11 November 2019; p. D012S138R002.
16. Wu, X.; Zhai, C.; Zheng, Y.; Chen, A.; Yu, X.; Xu, J.; Sun, Y.; Cong, Y.; Tang, W.; Liu, X. Effect of Different Salt Ions with Different Concentrations on the Stability of Carbon Dioxide-In-Water Foam Fracturing Fluids. *J. Mol. Liq.* **2023**, *373*, 121215. [CrossRef]
17. Zhao, J.; Wu, T.; Pu, W.; Daijun, D.; Chen, Q.; Chen, B.; Li, J.; Huang, Y. Application Status and Research Progress of CO_2 Fracturing Fluid in Petroleum Engineering: A Brief Review. *Petroleum* **2024**, *10*, 1–10. [CrossRef]
18. Pu, W.; Wu, T.; Zhao, J.; Gao, H.; He, M.; He, Y.; Chen, Y.; Zhu, Y. Nano-Structure of Hydrolyzed Polyacrylamide Strengthened Ultra Stable Nitrogen foam: Lab Experiments and Molecular Dynamics Simulation. *J. Mol. Liq.* **2024**, *396*, 124103. [CrossRef]
19. Liu, B.; Wang, Y.; Liang, L.; Zeng, Y. Achieving Solubility Alteration with Functionalized Polydimethylsiloxane for Improving the Viscosity of Supercritical CO_2 Fracturing Fluids. *RSC Adv.* **2021**, *11*, 17197–17205. [CrossRef] [PubMed]
20. Hu, D.; Sun, S.; Yuan, P.-Q.; Zhao, L.; Liu, T. Exploration of CO_2-Philicity of Poly(Vinyl Acetate-*Co*-Alkyl Vinyl Ether) through Molecular Modeling and Dissolution Behavior Measurement. *J. Phys. Chem. B* **2015**, *119*, 12490–12501. [CrossRef]
21. Hoover, W.G. Canonical Dynamics: Equilibrium Phase-Space Distributions. *Phys. Rev. A* **1985**, *31*, 1695–1697. [CrossRef]
22. Berendsen, H.J.C.; Postma, J.P.M.; Van Gunsteren, W.F.; DiNola, A.; Haak, J.R. Molecular Dynamics with Coupling to an External Bath. *J. Chem. Phys.* **1984**, *81*, 3684–3690. [CrossRef]
23. Karasawa, N.; Goddard, W.A. Acceleration of Convergence for Lattice Sums. *J. Phys. Chem.* **1989**, *93*, 7320–7327. [CrossRef]
24. Kong, W.; Lv, B.; Jing, G.; Zhou, Z. How to Enhance the Regenerability of Biphasic Absorbents for CO_2 Capture: An Efficient Strategy by Organic Alcohols Activator. *Chem. Eng. J.* **2022**, *429*, 132264. [CrossRef]
25. Wu, H.; Zhang, X.; Xu, D.; Li, B.; Jiang, Z. Enhancing the Interfacial Stability and Solvent-Resistant Property of PDMS/PES Composite Membrane by Introducing a Bifunctional Aminosilane. *J. Membr. Sci.* **2009**, *337*, 61–69. [CrossRef]
26. Tubman, N.M.; Liberatore, E.; Pierleoni, C.; Holzmann, M.; Ceperley, D.M. Molecular-Atomic Transition along the Deuterium Hugoniot Curve with Coupled Electron-Ion Monte Carlo Simulations. *Phys. Rev. Lett.* **2015**, *115*, 045301. [CrossRef] [PubMed]
27. Zhang, G.; Wu, T.; Li, J.; Pang, Q.; Yang, H.; Liu, G.; Huang, H.; Zhu, Y. Dynamics Simulation of the Effect of Cosolvent on the Solubility and Tackifying Behavior of PDMS Tackifier in Supercritical CO_2 Fracturing Fluid. *Colloids Surf. Physicochem. Eng. Asp.* **2023**, *662*, 130985. [CrossRef]
28. Dai, X.; Guo, Z.; Liu, W. Ultraviolet-Driven Janus Foams with Wetting Gradients: Unidirectional Penetration Control for Underwater Bubbles. *ACS Appl. Mater. Interfaces* **2022**, *14*, 42734–42743. [CrossRef]
29. Myers, D. *Surfaces, Interfaces, and Colloids: Principles and Applications*, 1st ed.; Wiley: Hoboken, NJ, USA, 2002; ISBN 978-0-471-33060-8.
30. Monsalve, A.; Schechter, R.S. The Stability of Foams: Dependence of Observation on the Bubble Size Distribution. *J. Colloid Interface Sci.* **1984**, *97*, 327–335. [CrossRef]
31. Zhang, Y.; Song, H.; Li, D.; Zhang, L.; Yang, C.; Li, X.; Ren, X. Experiment on High Pressure CO_2 Foam Stability of Nonionic Surfactants. *J. China Univ. Pet.* **2013**, *37*, 119–123+128.
32. Jing, J.; Sun, J.; Zhang, M.; Wang, C.; Xiong, X.; Hu, K. Preparation and Rheological Properties of a Stable Aqueous Foam System. *RSC Adv.* **2017**, *7*, 39258–39269. [CrossRef]
33. Zhai, Y.; Gao, Y.; Jiang, W.; Yi, W. Effects of Surfactants with Different HLB Values on $LiNi_{0.8}Co_{0.1}Mn_{0.1}O_2$. *Mater. Rep.* **2023**, *37* (Suppl. S1), 24–26.
34. Lin, Z.; Xu, F.; Wang, L.; Hu, L.; Zhu, L.; Tan, J.; Li, Z.; Zhang, T. Characterization of Oil Component and Solid Particle of Oily Sludge Treated by Surfactant-Assisted Ultrasonication. *Chin. J. Chem. Eng.* **2021**, *34*, 53–60. [CrossRef]
35. Alex, M.; Kareth, S.; Petermann, M. Stability of Emulsions in Presence of Compressed Propane. *J. Supercrit. Fluids* **2012**, *66*, 282–290. [CrossRef]
36. Huang, Q.; Wang, M.; Zhang, C.; Wang, Z.; Liu, B.; Lu, Z. Irritation and Interfacial Properties of Glucose Ester Surfactant. *J. South China Univ. Technol. (Nat. Sci. Ed.)* **2021**, *49*, 8–15.
37. Luo, Z.; Su, Y.; Yue, S.; Yu, Q.; Tursun, R.; Zhang, J. Effect of Fluorocarbon Surfactant on Electroforming of Copper Nano-Powders. *Int. J. Electrochem. Sci.* **2021**, *16*, 210232. [CrossRef]